

NUMERICAL INVESTIGATION INTO THE EFFECTS OF TURBULENCE MODELLING ON THE AEROELASTIC ANALYSIS OF FLEXIBLE WINGS

Thomas B. Goonan¹, Rui P. R. Cardoso¹, Oluwamayokun B. Adetoro¹

¹Department of Mechanical and Aerospace Engineering,

Brunel University London,

Uxbridge, UB8 3PH, UK

Thomas.Goonan2@brunel.ac.uk

Rui.Cardoso@brunel.ac.uk

Mayo.Adetoro@brunel.ac.uk

Keywords: Aeroelasticity, CFD, Turbulence Modelling, Detached Eddy Simulation.

Abstract: As wings are becoming more flexible, existing aeroelastic analysis methods may struggle to accurately resolve the complex flow around oscillating wings. A numerical case study is performed to compare the aeroelastic predictions obtained for a wing with two degrees of freedom when turbulence models of varying fidelity are used. Results are presented and compared in the time and frequency domain for simulations using Reynolds Averaged Navier Stokes and Detached Eddy turbulence models. These results show significant differences between the results obtained, particularly in the time domain. The numerical methodology, setup and results for this case study are presented in this paper.

1 INTRODUCTION

Increasing the aspect ratio of a wing is one of the fundamental methods for improving the aerodynamic efficiency of an aircraft. This has obvious benefits for the endurance, range and fuel economy of an aircraft and has led to the adoption of high aspect ratio wings for aircraft requiring extreme aerodynamic performance such as gliders and High Altitude Long Endurance (HALE) aircraft. One of the drawbacks of increasing the aspect ratio is the increased structural weight compared to an equivalent low or moderate aspect ratio wing of similar flexibility. To counter this, the wing can be designed to be more flexible which reduces the weight of the structure. As the wing becomes more flexible, the tip deflection under aerodynamic loading will also increase which has the advantage of increasing the effective dihedral, but also increases the wings susceptibility to aeroelastic phenomena. This has caused issues for aircraft utilising lightweight structures in the past including the NASA Helios aircraft which broke up mid-air after excessive dihedral caused rapid pitch fluctuations and the aircraft exceeded its maximum airspeed which led to structural failure. One of the fundamental causes of this incident was identified as the insufficient modelling of the aeroelastic phenomena encountered by such an aircraft, [1].

Traditionally, linear approximations such as potential flow and panel methods have been coupled with structural solvers to model the aeroelastic performance of a wing. This approach has worked well for relatively rigid wings which do not experience any non-linear aerodynamic effects such as flow separation or shock formation. More advanced aerodynamic solvers which

solve the Navier-Stokes equations are now being used in aeroelastic analysis tools, particularly for high speed flows where the incompressible methods are unable to predict shock formation.

For low speed applications, the majority of recent work still relies on panel methods. For more traditional wings, these methods are still valid, if not ideal, and the computational cost of more accurate analysis is prohibitive. However, for high aspect ratio, flexible wings, the use of panel methods severely limits the range of conditions that can be considered. For example, Carre and Palacios, [2], limit the optimisation boundaries so that non-linear effects such as flow separation cannot occur. Hewson, [3], has used stall modelling to improve the accuracy of the panel method for such cases but there is still considerable computational cost involved in developing these stall models.

Changing from inviscid to viscous Computational Fluid Dynamics (CFD) has been shown to increase the accuracy of predictions for aeroelastic simulations, [4], [5]. The majority of CFD solvers solve the Reynolds Averaged Navier-Stokes (RANS) equations which average turbulent fluctuations to predict the turbulent energy within the flow. These solvers perform well for steady flows such as the attached flow over an aerofoil but the accuracy is limited for transient simulations due to the dependence of a transient flow on the development of the flow.

Large Eddy Simulation (LES) models resolve the majority of turbulence within the flow. These large turbulent eddies are responsible for the majority of energy and momentum transport. Only the smallest of eddies, determined by a filter equation, are modelled with a sub-grid model as these are assumed to be isotropic and therefore easier to model. A much more refined grid is required for LES models compared to RANS, especially in the boundary layer where extremely fine grids are required for moderate or high Reynolds number flows. Therefore, the computational cost of LES is orders of magnitude larger than RANS.

Detached Eddy Simulation (DES) models are a compromise between RANS and LES. RANS equations are used for the boundary layer where the flow is stable and relatively steady. The turbulence model changes from RANS to LES when the flow separates to improve the accuracy of the predictions. The computational grids required for DES turbulence models are far more complicated than those for RANS or LES due to varying requirements depending on the flow conditions, however, for aeroelastic simulations where the effects of flow separation have a significant effect on the results, DES models offer a compromise between the accuracy of LES and the computational efficiency of RANS.

This paper will present a case study comparing the results of a FSI simulation using RANS and DES turbulence models. The purpose of this study is to compare the accuracy of RANS and DES to the LES simulations carried out by De Nayer et al, [6] and the corresponding experimental study by Wood et al, [7].

2 FORMULATION

This section describes the governing equations for the fluid and structural dynamics which are solved for this paper. The coupling method for the Fluid Structure Interaction (FSI) coupling is also explained here.

2.1 Computational Fluid Dynamics (CFD)

The conservation of momentum within a fluid is governed by the Navier-Stokes equation which is given below for direction x :

$$\frac{\partial(\rho u)}{\partial t} + \nabla \cdot (\rho u \mathbf{u}) = -\frac{\partial p}{\partial x} + \nabla \cdot (\mu \nabla u) + S_M \quad (1)$$

where, u is the velocity component in the x direction, \mathbf{u} is the velocity vector, and μ is the dynamic viscosity of the fluid. S_M is the external source of momentum. The RANS formulation assumes that the various terms can be decomposed into a mean term and a fluctuation. For example, the velocity will have a mean, \bar{u} , and fluctuation u' such that, $u = \bar{u} + u'$. The RANS governing equation for momentum conservation is:

$$\frac{\partial \bar{\rho} \bar{u}}{\partial t} + \nabla \cdot (\bar{\rho} \bar{u} \bar{\mathbf{u}}) + \nabla \cdot (\overline{\bar{\rho} u' \mathbf{u}'}) = -\frac{\partial \bar{p}}{\partial x} + \nabla \cdot (\mu \nabla \bar{u}) + S_M \quad (2)$$

This equation results in six new terms known as the Reynolds Stresses which arise from the average of the product of the velocity fluctuations. The different RANS turbulence models vary in their approach to calculating these Reynolds stresses, but the majority of two equation models such as the one used for this paper utilise the Boussinesq equation shown below:

$$\tau_{ij} = -\overline{\rho u'_i u'_j} = \mu_t \left(\frac{\partial \bar{U}_i}{\partial x_j} + \frac{\partial \bar{U}_j}{\partial x_i} \right) - \frac{2}{3} \rho k \delta_{ij} \quad \text{for } i, j = 1-3 \quad (3)$$

where μ_t is the eddy viscosity and δ_{ij} is the Kronecker delta ($\delta_{ij} = 1$ if $i = j$ and $\delta_{ij} = 0$ if $i \neq j$). For the k - ω Shear Stress Transport (SST) turbulence model used for this paper, the eddy viscosity is found proportional to the turbulent kinetic energy, k , and turbulent specific dissipation rate, ω using the following equation:

$$\mu_t = \frac{a_1 \rho k}{\max(a_1 \omega, b_1 F_{23} S)} \quad (4)$$

where k , ω , F_{23} and a_1 and b_1 are found using the equations and coefficients described by Menter et. al., [8].

DES Models differ from RANS models as some of the turbulent eddies are resolved. This paper uses the Improved Delayed Detached Eddy Simulation (IDDES) variant of the k - ω SST model which was developed by Gritskevich et al, [9], as an extension to the Spalart-Allmaras IDDES formulation. The turbulent kinetic energy and turbulent specific dissipation rate are found using:

$$\frac{\partial \rho k}{\partial t} + \nabla \cdot (\rho \bar{u} k) = \nabla \cdot [(\mu + \sigma_k \mu_t) \nabla k] + P_k - \frac{\rho \sqrt{k^3}}{l_{IDDES}} \quad (5)$$

$$\frac{\partial \rho \omega}{\partial t} + \nabla \cdot (\rho \bar{u} \omega) = \nabla \cdot [(\mu + \sigma_\omega \mu_t) \nabla \omega] + 2(1 - F_1) \rho \sigma_{\omega 2} \frac{\nabla k \cdot \nabla \omega}{\omega} + \alpha \frac{\rho}{\mu_t} P_k - \beta \rho \omega^2 \quad (6)$$

The eddy viscosity is found in a similar manner as that for the RANS formulation using:

$$\mu_t = \rho \frac{a_1 \cdot k}{\max(a_1 \cdot \omega, F_2 \cdot S)} \quad (7)$$

P_k in (5) is a turbulence production term and is found using:

$$P_k = \min(\mu_t S^2, 10 \cdot C_\mu \rho k \omega) \quad (8)$$

The IDDES length scale, l_{IDDES} , is defined as:

$$l_{IDDES} = \tilde{f}_d \cdot (1 + f_e) \cdot l_{RANS} + (1 - \tilde{f}_d) \cdot l_{LES} \quad (9)$$

where l_{LES} is defined by:

$$l_{LES} = C_{DES} \min(C_w \max[d_w, h_{max}], h_{max}) \quad (10)$$

and l_{RANS} by:

$$l_{RANS} = \frac{\sqrt{k}}{C_\mu \omega} \quad (11)$$

These length scales add a turbulent source term to (5) which allows the resolving of the eddies. The LES length scale is determined by the grid size through the term, h_{max} , which is the length of the longest edge in the cell. The LES length scale is therefore the minimum eddy size which will be resolved by (5) and (6) above. The full set of equations needed for this turbulence model have not been included here for brevity. These equations and the coefficients used in these equations can be found in the paper by Gritskevich et al, [9].

2.2 Computational Structural Dynamics (CSD)

The structural system is modelled using a simple two degree of freedom (DoF) spring-damper model which is the same as that used by De Nayer et al, [6]. This system is solved for each fluid time step to find the displacement and rotation of the aerofoil about its elastic axis. The displacement, Y , and rotation θ are described by:

$$m\ddot{Y} + C_t\dot{Y} + K_t Y = F_{EXT} + x_{CG}m\ddot{\theta} + y_{CG}m\dot{\theta}^2 \quad (12)$$

$$I\ddot{\theta} + C_r\dot{\theta} + K_r\theta = M_{EXT} + x_{CG}m\ddot{Y} \quad (13)$$

where m is the mass of the aerofoil and I is the mass moment of inertia about the elastic axis. C_t , C_r , K_t and K_r are the damping and spring coefficients in the translational and rotational direction. x_{CG} and y_{CG} are the location of the centre of gravity relative to the elastic axis in the x and y directions as shown in figure 1.

The structural equations are solved using the Newmark-Beta method which discretises the equations with second order accuracy. The velocity and angular velocity for the current time, t , are found using:

$$\dot{Y}^t = \dot{Y}^{t-\Delta t} + \Delta t \left[(1 - \gamma)\ddot{Y}^{t-\Delta t} + \gamma\ddot{Y}^t \right] \quad (14)$$

$$\dot{\theta}^t = \dot{\theta}^{t-\Delta t} + \Delta t \left[(1 - \gamma)\ddot{\theta}^{t-\Delta t} + \gamma\ddot{\theta}^t \right] \quad (15)$$

where Δt is the size of the time step. The displacement and rotation are found using:

$$Y^t = Y^{t-\Delta t} + \frac{1}{2}\Delta t^2 \left[(1 - 2\beta)\ddot{Y}^{t-\Delta t} + 2\beta\ddot{Y}^t \right] \quad (16)$$

$$\theta^t = \theta^{t-\Delta t} + \frac{1}{2}\Delta t^2 \left[(1 - 2\beta)\ddot{\theta}^{t-\Delta t} + 2\beta\ddot{\theta}^t \right] \quad (17)$$

The discretised structural equations are given by:

$$m\ddot{Y}^t + C_t\dot{Y}^t + K_tY^t - x_{CG}m\ddot{\theta}^{t-\Delta t} - y_{CG}m(\dot{\theta}^{t-\Delta t})^2 = F_{EXT}^t \quad (18)$$

$$I\ddot{\theta}^t + C_r\dot{\theta}^t + K_r\theta^t - x_{CG}m\ddot{Y}^{t-\Delta t} = M_{EXT}^t \quad (19)$$

These equations are solved using values of 0.5 and 0.25 for γ and β , respectively. With these values, the solution will be unconditionally stable.

2.3 FSI Coupling

The fluid and structural equations are coupled using an explicit scheme where the segregated equations are solved sequentially. An implicit scheme could also be used but would offer little improvement in accuracy due to the small time steps used in this case and would result in a large increase in computational cost. The fluid equations are first solved to find the forces and moments acting on the wing about its elastic axis. The forces and moments are transferred to the structural solver and the displacement and rotation calculated using (14) to (19). As these are calculated for the elastic axis, the displacement of each face on the fluid grid must be found. For a rigid body, this is simplified by using a cylindrical coordinate system with its central axis along the wing's elastic axis as shown in figure 2. The location of point P after the wing displaces by distance Y and rotates by angle θ can be found using:

$$P_x = -|r| \cos(\lambda + \theta) \quad (20)$$

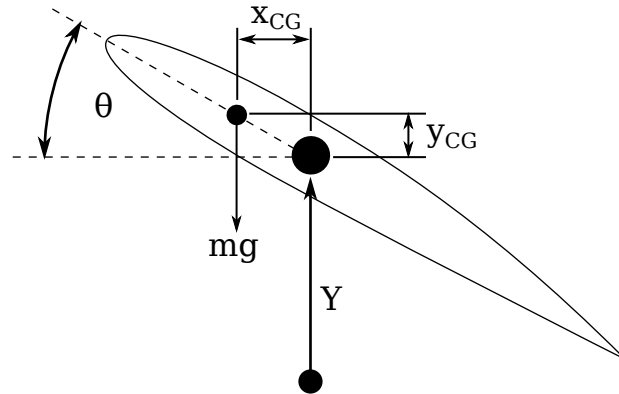


Figure 1: The coordinate system used for the structural system.

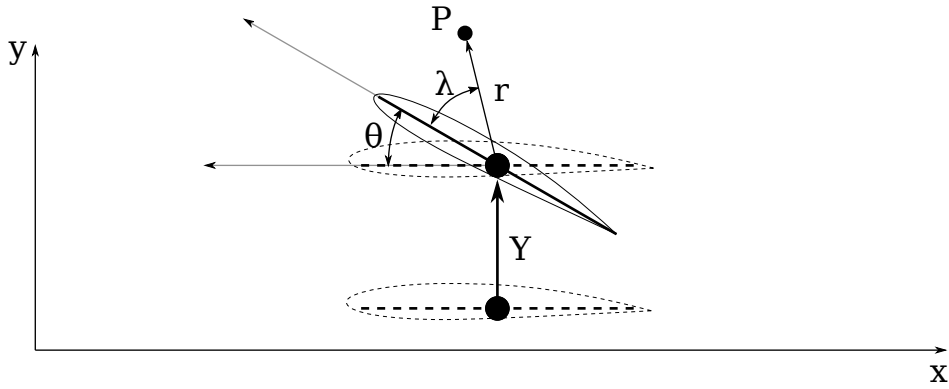


Figure 2: The coordinate system used to calculate the displacement of point P as the wing moves.

$$P_y = |r| \sin(\lambda + \theta) + Y \quad (21)$$

The values for r and λ are found at the start of the simulation and can be kept constant for a rigid body. The current location of any face centre can then be found using (20) and (21). The displacement of each face centre is used as a boundary condition for the Laplacian solver used to update the mesh. This mesh motion solver is one of the default OpenFOAM solvers and the diffusivity increases with distance from the wall.

3 CASE STUDY

The case considered for this paper is a rigid wing with two degrees of freedom at a Reynolds number of 36,000. This case is based on the experimental and numerical study performed by Wood et al, [6] [7]. Two simulations are considered for this study, the first using the $k-\omega$ SST RANS model and the second using the $k-\omega$ SST IDDES DES model. The numerical setup and results of these simulations are discussed in this section.

3.1 CFD Setup

Both simulations are performed on C-grids with appropriate refinement for the turbulence model used. The grid used for RANS simulation comprises of 1 M cells. The grid requirements for DES modelling result in a much finer grid of 3 M cells. This mesh is shown in figure 4. Both grids are designed to have a first layer height which results in a y^+ of less than 1. A comparison of the two grids is shown in figure 3.

For both simulations, a pressure far-field boundary condition was imposed 20 chord lengths away from the wing surface and a symmetry boundary condition constrains the front and back faces. A time step size of $1e-5$ s and $2e-6$ s is used for the RANS and DES simulation to ensure

Table 1: Parameters used for the CFD simulations.

Parameter	Description	Value	Unit
U	Velocity	5.37	m/s
P	Pressure	101325	Pa
T	Temperature	288	K
Re	Reynolds Number	36000	

that the maximum Courant number remains less than 1 for the entire domain. The wing is at zero angle of attack and the freestream conditions are given in table 1. The wing model used in the experiment had a span of 0.5 m. To reduce the computational expense of the simulations, particularly for the DES model, the wing modelled in CFD had a span of 0.025 m and the forces and moments are scaled before being passed to the structural solver.

The CFD equations are solved using the OpenFOAM fluid dynamics solver. All spatial discretisation is second order accurate and the time discretisation utilised the Crank-Nicholson second order accurate scheme.

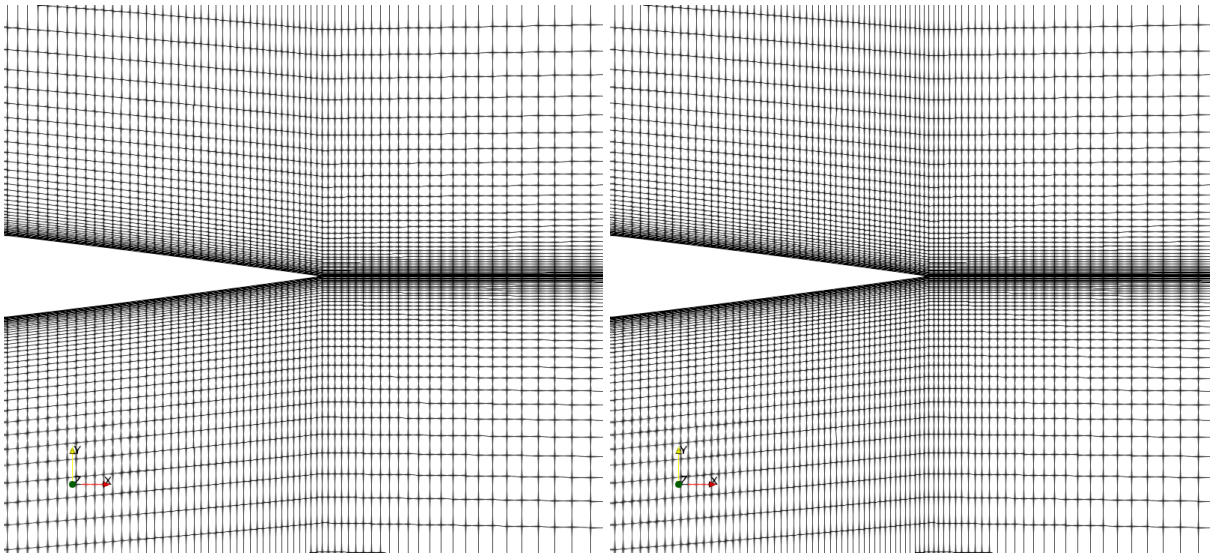


Figure 3: The grid spacing near the trailing edge used for the RANS (left) and DES (right) simulations.

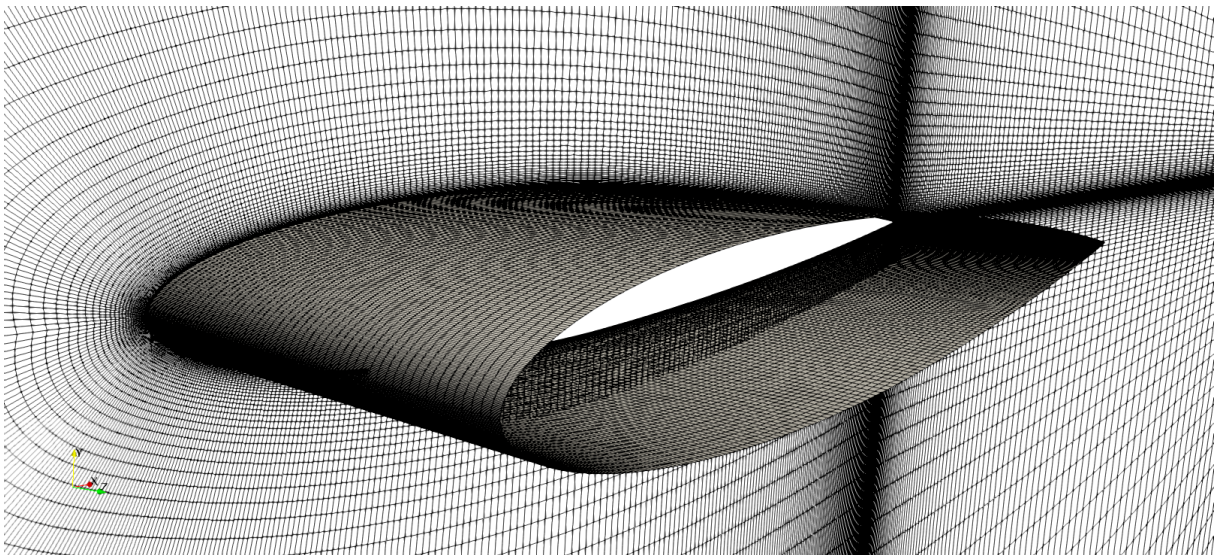


Figure 4: The grid used for DES simulations.

3.2 Structural and FSI Setup

The structural equations are implemented as a function object within OpenFOAM. These are solved for each time-step using the forces and moments calculated on the wing surface. The mechanical properties used for this case are shown in table 2.

Table 2: Mechanical properties used in the simulations.

Parameter	Description	Value	Unit
EA	Position of the EA relative to leading edge	0.017	m
e_{CG}	Distance between EA and CoG	0.0006	m
m	Mass	0.33521	kg
I	Inertia	1.38e-4	kg m ²
K_t	Bending stiffness	705	N/m
K_r	Torsional stiffness	0.3823	Nm/rad
C_t	Translational damping	7.07e-2	Ns/m
C_r	Rotational damping	1.67e-5	Nm/s

In the experiment carried out by Wood et al, [7], the wing was not excited during the test. However, for a numerical simulation, some form of excitation is required to speed up the development of the oscillations. While the numerical and experimental results cannot be compared in the time domain due to the use of an initial excitation, without this, the simulation would need to be run for an excessively long time before any significant oscillations would occur. For this case study the flow is allowed to develop for 0.1 s before the wing is released with an initial vertical velocity of 0.05 m/s. The simulations are both run for 1 second of FSI simulation.

3.3 Results

The RANS and DES simulations are run using the setup described in the previous section. The point P_w , which is located on the aerofoil surface at 70% of its chord, is monitored during the experiments performed by Wood et al, [7], and this point was found to flutter with a frequency of 7.79 Hz. The vertical displacement of this point over time as predicted by the RANS and DES simulations is shown in figure 5. As the initial conditions of the simulations cannot be the same as those for the experiment, a direct comparison between the simulations and experiment in the time domain is not possible. Instead, a Fast Fourier Transform (FFT) of the displacement and rotation is performed to find the dominant frequencies. The results of this FFT are also shown in figure 5. Due to the relatively short time resolved during these simulations, the frequency resolution of the FFT analysis is limited which adds some uncertainty to the results. Despite this it is clear that both the RANS and DES models predict a frequency of oscillation similar to that of the experiment with oscillation frequencies of 7.00 Hz and 7.60 Hz, respectively. However, unlike the experiment, the amplitude of the displacement for the RANS simulation appears to be decaying rather than increasing as would be expected for a wing which is experiencing flutter. The DES predicted frequency is almost identical to that predicted by the LES simulation performed by De Nayer et al, [6].

Figure 6 shows the displacement and rotation of the wing's elastic axis over time. As the amplitudes of the displacement and rotation for the DES model are increasing with time, it is clear that the DES results show flutter occurring. However the RANS results show the displacement decreasing while the rotation amplitude is slowly increasing. This could be due to the phase difference between the displacement and rotation as the rotation has a relatively large effect on the forces experienced by the aerofoil. This could be misleading as even after a significant flow time has been resolved, the RANS simulation appears to be stable and would only appear unstable once the displacement and rotation are in phase.

Figure 7 shows the forces and moments acting on the wing. This clearly shows that the amplitude of the vertical force and moment in the RANS simulation is decreasing over time. The

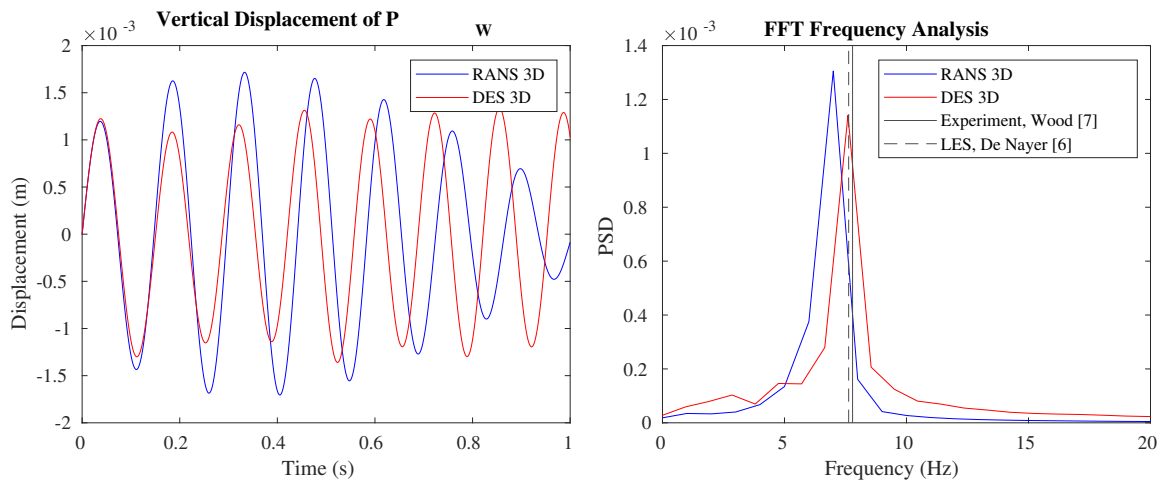


Figure 5: The displacement of point P_w over time and in the frequency domain.

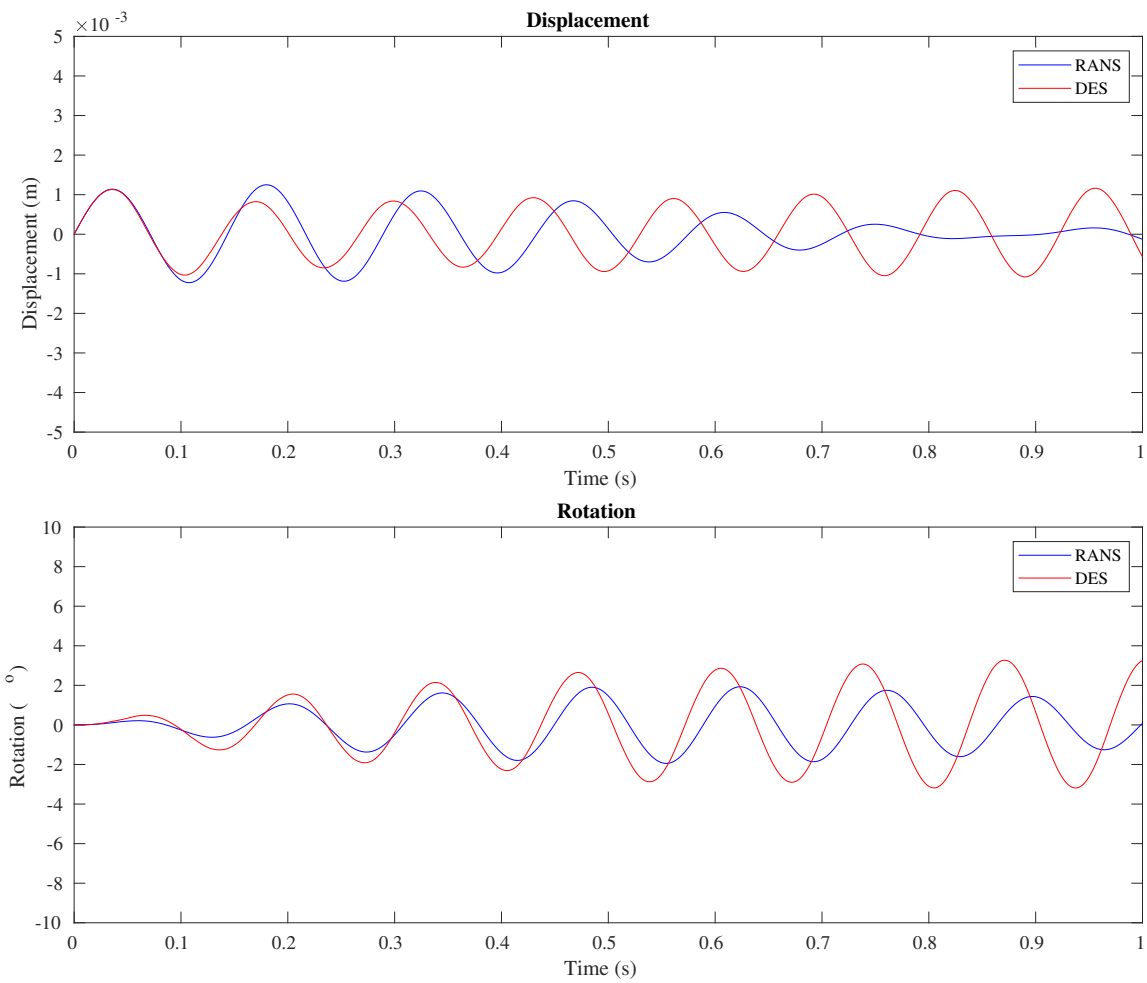


Figure 6: The displacement and rotation of the wing over time.

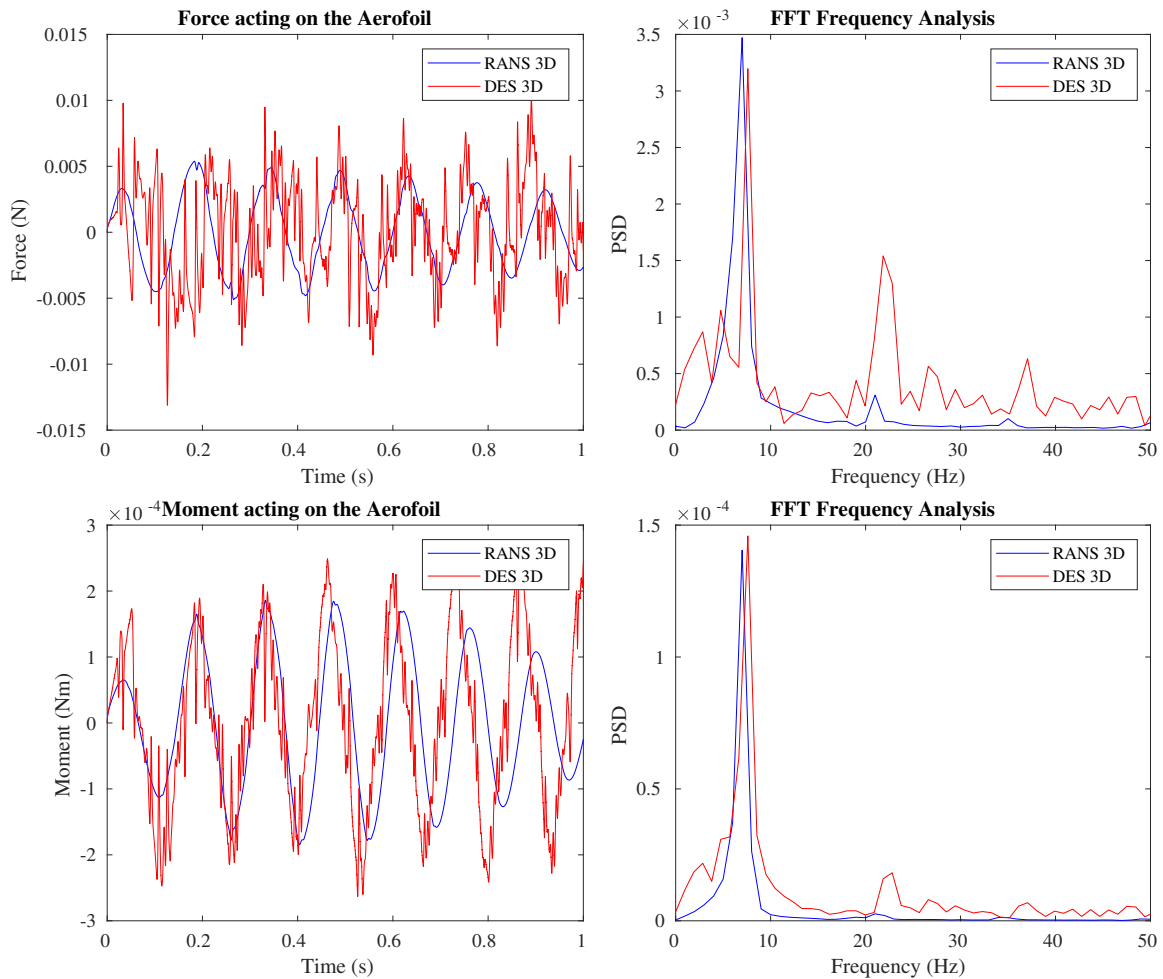


Figure 7: The force and moment acting on the wing over time and in the frequency domain.

main frequencies for the force and moments are similar to those of the displacement and rotation. However, comparing the RANS and DES results, the DES forces and moments also include a second frequency which is not present in the RANS results. This second frequency is likely due to the resolving of the turbulent eddies in the flow particularly in areas of flow separation which occur due to the motion of the wing. This separation can be seen in the pressure and velocity fields which are shown in figures 8 and 9 for one period of oscillation. These highlight the differences between the RANS and DES models, particularly in the wake and in the areas of separated flow behind the aerofoil. Looking at the velocity field, it is clear that the flow is separated over a significant portion of the aerofoil. Due to the averaging of the turbulent fluctuations in the RANS model, these models are incapable of resolving the complex flow which is apparent in the DES results. This is also apparent in the wake behind the aerofoil where there are no signs of vortices being shed into the wake of the aerofoil in the RANS simulation. The effect of the averaging of the velocity field is shown in the pressure field where the RANS model has failed to capture the pressure fluctuations shown by the DES model. The effect of the pressure fluctuations can be seen in the forces and moments acting on the wing. While these have a relatively small effect on a rigid wing, their effect will be larger on flexible wings, particularly when the skins used are thin and flexible such as those used on HALE aircraft. This will likely induce extra stresses on the wing which are not modelled by the RANS simulations.

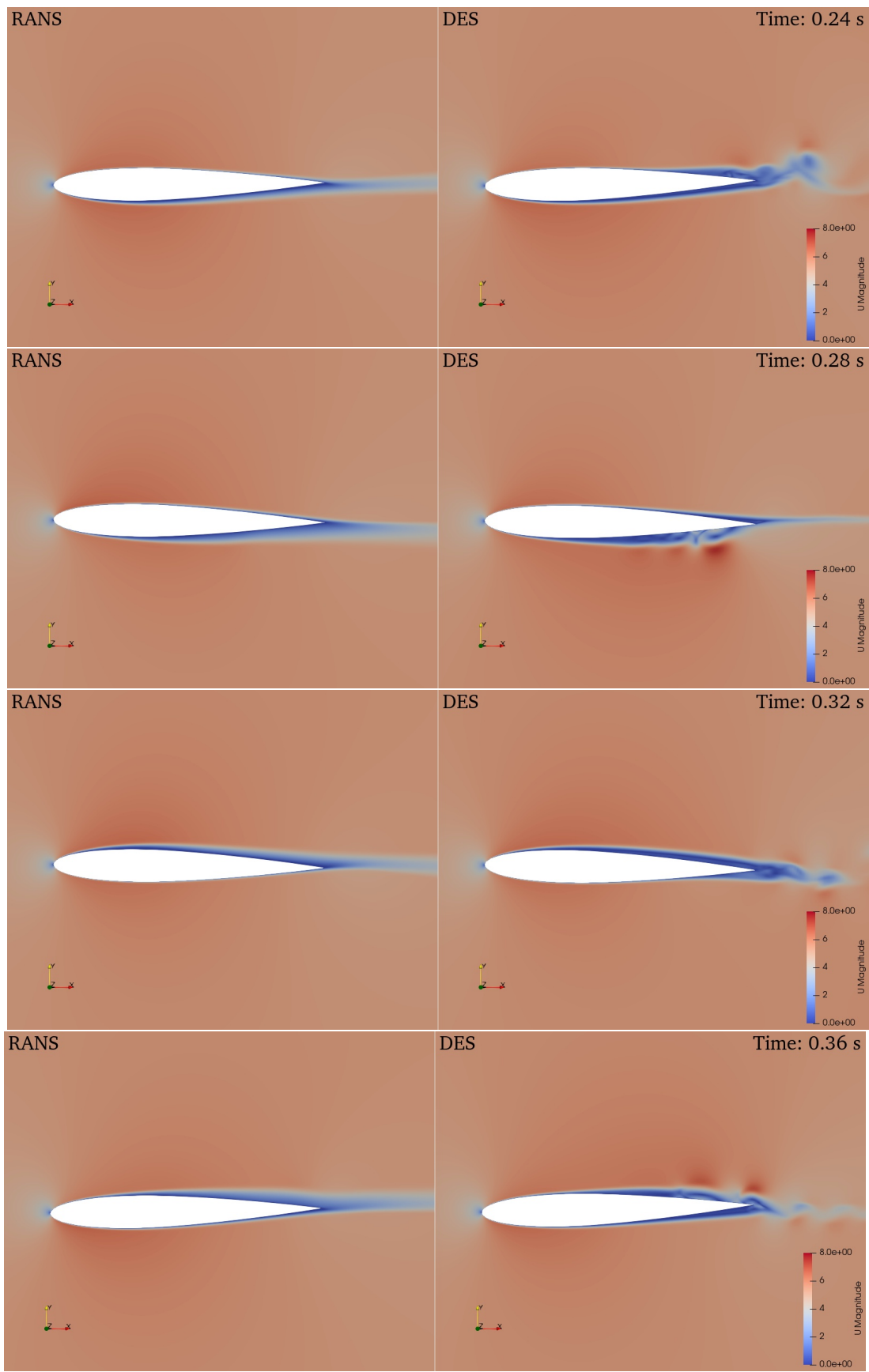


Figure 8: The velocity field in the fluid surrounding the aerofoil.

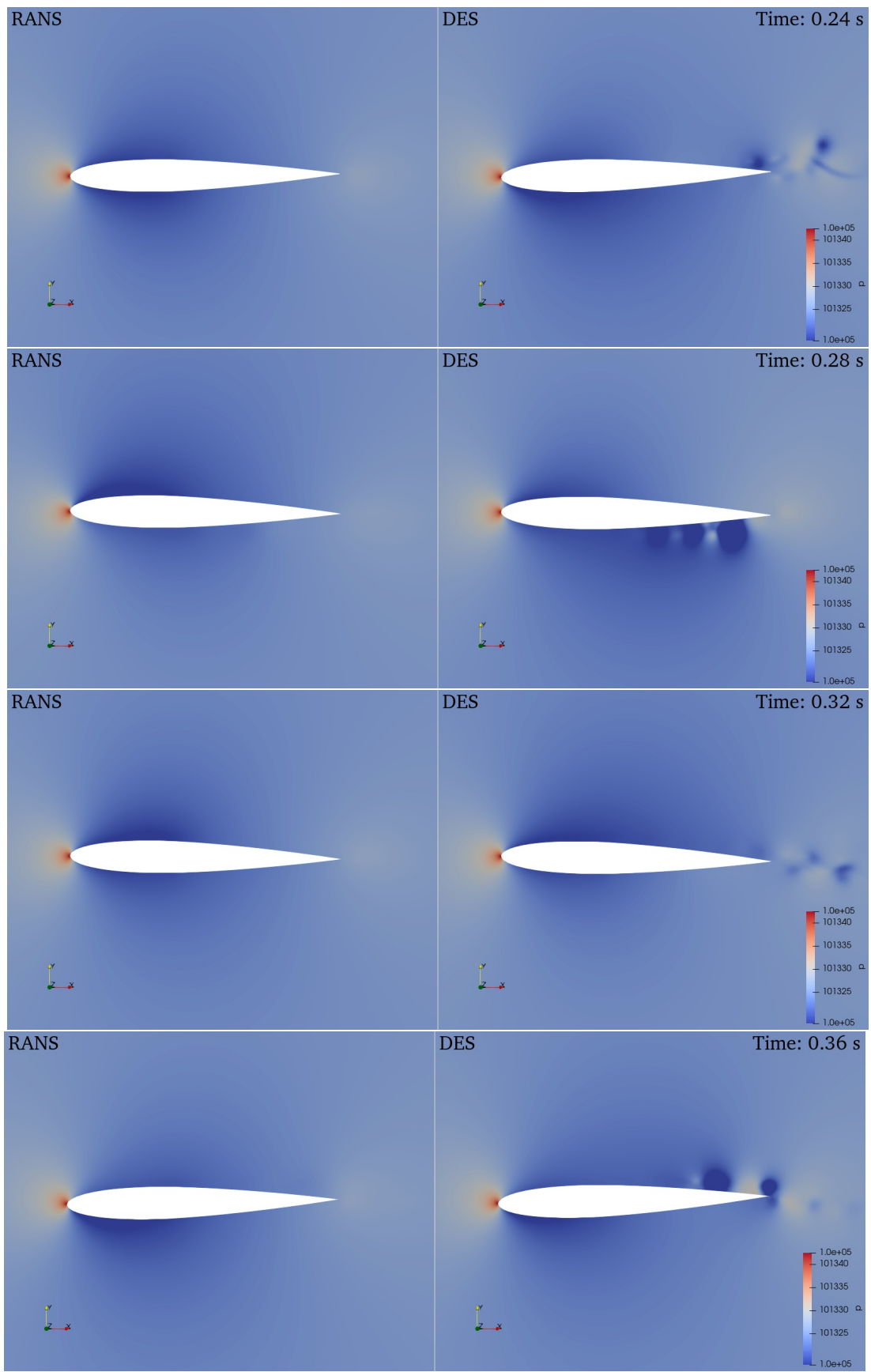


Figure 9: The pressure in the fluid surrounding the aerofoil.

4 CONCLUSIONS

A case study comparing the results from FSI simulations using a RANS and DES turbulence model has been performed. These simulations clearly show that there are significant differences between the results of the RANS and DES simulations and indicate that the turbulence model may have a significant impact on the results obtained when performing an aeroelastic simulation of a flexible wing. The RANS model gave reasonable prediction of the flutter frequency of the wing, however, its predictions of the amplitude of oscillation are not as good as those of the DES model. This is balanced by the computational efficiency of the RANS model compared to the DES model due to the coarser grid requirements for RANS simulations and the larger time step which can therefore be used.

The DES model is shown to be a reasonable compromise between the accuracy of LES and the computational efficiency of RANS models. The frequency predicted by the DES model is as close to the experimental results as the LES results and better than the RANS model. This model has been shown to resolve the complex flow structures that occur as the wing moves which affect the forces and moments acting on the wing. The resolving of the wake after the wing is also much improved over the RANS model which could affect the aeroelastic analysis of aircraft components lying in the wing's wake such as the horizontal stabilizer.

The main disadvantage of the DES model is the computational cost which was significantly greater than for the RANS simulation. The RANS simulation used approximately 1100 core hours to complete while the DES required 2600 core hours. A direct comparison between the RANS and DES simulations is not possible as these were performed on computers with different specifications. A second disadvantage is the more complex meshing which requires the user to have an understanding of the methodology behind the DES formulation so that the turbulent flow structures are resolved.

5 REFERENCES

- [1] Noll, T. E., Brown, J. M., Perez-Davis, M. E., et al. (2004). *Investigation of the Helios Prototype Aircraft Mishap*. NASA Langley Research Center.
- [2] Carre, A. and Palacios, R. (2019). Low-altitude dynamics of very flexible aircraft. In *AIAA SciTech 2019 Forum, January 2019, San Diego, California*.
- [3] Hewson, W. (2019). *A New Aerodynamic Model for Unsteady Separated Flow on High Aspect Ratio Flexible Wings*. Ph.D. thesis, University of Bristol, UK.
- [4] Heeg, J. and Chwalowski, P. (2019). Predicting transonic flutter using nonlinear computational simulations. In *International Forum on Aeroelasticity and Structural Dynamics*.
- [5] Šekutkovski, B., Kostić, I., Simonović, A., et al. (2016). Three-dimensional fluid–structure interaction simulation with a hybrid rans–les turbulence model for applications in transonic flow domain. *Aerospace Science and Technology*, 49.
- [6] De Nayer, G., Breuer, M., and Wood, J. N. (2020). Numerical investigations on the dynamic behavior of a 2-dof airfoil in the transitional re number regime based on fully coupled simulations relying on an eddy-resolving technique. *International Journal of Heat and Fluid Flow*, 85.

- [7] Wood, J. N., Breuer, M., and De Nayer, G. (2020). Experimental investigations on the dynamic behavior of a 2-dof airfoil in the transitional re number regime based on digital-image correlation measurements. *Journal of Fluids and Structures*, 96.
- [8] Menter, F. R., Kuntz, M., and Langtry, R. (2003). Ten years of industrial experience with the sst turbulence model. *Proceedings of the fourth international symposium on turbulence, heat and mass transfer*, 625–632.
- [9] Gritskevich, M. S., Garbaruk, A. V., Schütze, J., et al. (2012). Development of ddes and iddes formulations for the $k-\omega$ shear stress transport model. *Flow, turbulence and combustion*, 88(3), 431–449.

COPYRIGHT STATEMENT

The authors confirm that they, and/or their company or organization, hold copyright on all of the original material included in this paper. The authors also confirm that they have obtained permission, from the copyright holder of any third party material included in this paper, to publish it as part of their paper. The authors confirm that they give permission, or have obtained permission from the copyright holder of this paper, for the publication and distribution of this paper as part of the IFASD-2022 proceedings or as individual off-prints from the proceedings.